

Microfluidic Wound Model for Studying the Behaviors of *Pseudomonas aeruginosa* in Polymicrobial Biofilms

Evan Wright, Suresh Neethirajan, Xuan Weng

BioNano Laboratory, School of Engineering, University of Guelph, Guelph, Canada N1G 2W1; telephone: 1-519-824-4120 ext: 53922; fax: 1-519-836-0227; e-mail: sneethir@uoguelph.ca

ABSTRACT: *Pseudomonas aeruginosa* is a particularly problematic opportunistic pathogen due to its capacity to form recalcitrant biofilm structures, while cohabiting with other harmful/pathogenic species and harboring the capability to release toxins that cause tissue necrosis. Although it is now recognized that the majority of biofilm infections are polymicrobial, little is known about the complex interactions that occur within polymicrobial communities and few tools exist for studying these interactions. In this study, we have designed a microfluidic model that mimics the relevant physiological properties of wound microenvironment, while incorporating materials present in the human extracellular matrix/wound environment. Using microfluidics combined with imaging techniques, we have validated the robustness of our model comparing traditional GFP-tagging to new fluorescent staining techniques to visualize/resolve individual species within a polymicrobial habitat. We have also demonstrated that chemotactic stimuli may be incorporated into our model through specialized ports in our chamber. Our system is specifically designed for use with high resolution imaging techniques, allowing for data collection throughout the life of the biofilm and in real-time. Ultimately, this model can be used to investigate the spatio-temporal mechanobiological structures of the wound environment, and the response of the bacteria to the drug transport which will significantly contribute to our understanding of the development and progression of polymicrobial biofilm infections.

Biotechnol. Bioeng. 2015;112: 2351–2359.

© 2015 Wiley Periodicals, Inc.

KEYWORDS: in vitro wound models; microfluidics; chemotaxis; drug transport

Introduction

Pseudomonas aeruginosa is a uniflagellar (Taylor and Buckling, 2010) Gram-negative bacterium that is well known for its propensity to colonize wound sites, including burns and wounds, to cause severe eye infections, and to significantly contribute to the morbidity in the

cystic fibrosis patient population (Lockett et al., 2012). *P. aeruginosa's* pervasive roles in a variety of infections combined with accentuated antibiotic resistance during biofilm growth make this organism a significant threat to the medical community. Of its many virulence attributes, biofilm formation is a chief contributor to the recalcitrance of *P. aeruginosa* wound infections (Turner et al., 2014). Upon infection, *P. aeruginosa* rapidly aggregates to form microcolonies and adheres to surfaces, all while secreting copious amounts of extracellular polymeric substances that facilitate/enhance aggregation and adherence and simultaneously shelter the resulting biofilm from inimical assaults (Flemming and Wingender, 2010; Phillips et al., 2010). The resulting biofilm is often composed of multiple species and genotypes of bacteria, which can both compete and collaborate with one another as dictated by environmental pressures (e.g., nutrient source and availability, presence of oxidative or antimicrobial stress, etc.) (Phillips et al., 2010).

Synergistic interactions between species in polymicrobial biofilms can directly affect biovolume and functionality, as well as short term evolution (e.g., genetic recombination/acquisition of resistance genes) and virulence (Jiricny et al., 2014). We propose that an enhanced understanding of such community behaviors will lead to the identification of novel and specific targets for the control of biofilm infections. In order to understand the sum of polymicrobial interactions, one must first examine the parts of the whole, specifically the cellular characteristics of individual cells on an isolated level. Evaluating the swimming speed, genomic composition, chemotactic sensitivity, and the metabolic abilities, of isolated bacterial cells can be used to address the impact of co-existence on these abilities and the relative contributions of these abilities to polymicrobial biofilm formation. Our model offers the standard benefits of a microfluidic device, which include the ability to use reduced sample volumes, which can be directly correlated with reduced reagent consumption and can be scaled to encompass screening applications (e.g., antimicrobial susceptibility testing) (Sackmann et al., 2014). This model streamlines complex assay protocols, while more accurately mimicking the biological micro-environment than traditional assays, enabling precise control of the chemical environment, and the simultaneous recording of the subtle movements of individual biofilm cells at a high resolution (Sackmann et al., 2014; Wright et al., 2014). Agarose has been used to mimic the intrinsic properties of human tissue in various fields,

Conflict of interest: The authors declare no conflicts of interest.

Correspondence to: S. Neethirajan

Received 6 February 2015; Revision received 2 April 2015; Accepted 11 May 2015

Accepted manuscript online 20 May 2015;

Article first published online 6 July 2015 in Wiley Online Library

(<http://onlinelibrary.wiley.com/doi/10.1002/bit.25651/abstract>).

DOI 10.1002/bit.25651

including medical imaging (Taylor, 2006), biochemistry (Togunde et al., 2012), and microbiology (Tuson et al., 2012), and of critical importance, chemical diffusion through agarose is similar to that of tissue (Sirianni et al., 2008). Biofilm aggregates through culturing bacteria in a collagen gel matrix mimics the wound bed of chronic wounds (Werthen et al., 2010).

In addition to more accurately modeling a wound environment, we will show that our new model can be used to examine the chemotactic behaviors of organisms in our system in response to effectors, such as the amino acids arginine (Arg) and glutamine (Gln). Understanding the dynamic influence of these amino acids on *P. aeruginosa* may reveal a new therapeutic avenue that is natural, and therefore, may pose fewer toxic/systemic effects to the patient, all while potentially enhancing wound healing. With limited knowledge concerning individual cell/strain behaviors in polymicrobial wound infections we set out to: (i) demonstrate the viability of our newly designed wound model and non-invasive staining using agarose to mimic the physiological characteristics of human tissue, (ii) evaluate the effects of arginine and glutamine on the motility of *P. aeruginosa* cells in our system to better understand how they may influence cellular behaviour during a wound infection, and (iii) increase our understanding of the effects of polymicrobial interactions on *P. aeruginosa* through the initial characterization of differentially labeled dual-species biofilms of *P. aeruginosa* and *Escherichia coli*.

Materials and Methods

Bacterial Strains and Cell Culture

P. aeruginosa PAO1 wild type and a GFP-tagged strain were received as a gift from Dr. J.S. Lam of the University of Guelph. The GFP-expressing PAO1 strain tagged with EGFP in a mini Tn7 construct with a tetracycline resistance marker using the mini-CTX system for chromosomal integration of the GFP fluorophore. Bacteria were grown in tryptic soy broth (TSB; Sigma Chemical Co., St. Louis, MO) or on tryptic soy agar (TSA) plates at 37°C. One-tenth strength TSB was used for flow through biofilm experiments. Cell suspensions were prepared from overnight cultures grown in 5 mL TSB for biofilm imaging experiments. For cell migration quantification and motility experiments, a 100 μ L of the overnight culture was subcultured in 5 mL of fresh TSB incubated for 4 h. The cells were then harvested via centrifugation (SciLogex D3024, Berlin, CT) at 120 rcf for 3 min, the supernatant was discarded, and cells were resuspended in sterile distilled water. This was repeated two times and the cells were finally suspended in phosphate buffered saline (PBS). Wild type cells not expressing GFP were labeled with SYTO 9 green fluorescent nucleic acid stain (Invitrogen, Eugene, OR) before centrifugation for comparison to biofilms formed with the GFP-expressing strain. To make the dye solution, 3 μ L of dimethyl sulfoxide with 1.67 mM SYTO 9 dye and 1.67 mM propidium iodide was suspended in 1 mL water. Two hundred microliters of this dye solution was added to the washed cells (currently suspended in 1 mL water) to yield 1.2 mL of dyed cell solution. The staining solution was combined with the cell pellet and mixed thoroughly and kept in dark for 30 min.

Wound Model Creation

PDMS channels were initially designed using CAD software (AutoCAD 2013, Autodesk, Inc, San Rafael, CA) and printed onto transparency film with a high-resolution image setter (Fine Line Imaging, CO) to create the mask. The master mold for the PDMS layer was created using photolithography and SU-8 2000 photoresist epoxy (Microchem Corp, MA) following standard techniques (Whitesides et al., 2001). The silicon wafer was spin-coated (Brewer Science Cee200X Spin Coater, Rolla, MA) with a base layer of SU-8 and then heat treated to cure the epoxy. A second layer was added, cured, and then etched using a UV exposure system (UV-KUB, Kloé, France). Excess uncured photoresist was removed using the developing solution to reveal the completed master mold. Twenty grams of polydimethylsiloxane or PDMS elastomer base was mixed with 2 g of curing agent (Dow Corning Sylgard 184, Midland, MI), and the mixture was poured over the top of the silicon master mold. The solution was desiccated and then baked in an oven at 60°C to harden the PDMS. The device was cut free of the mold using a scalpel, and the inlet and outlet holes for the three channels were punched (Harris Uni-Core 0.75 mm, Sigma Chemical Co., St. Louis, MO).

A 3% gel was prepared using certified megabase agarose (Bio-Rad, Hercules CA). The mixture was microwaved for 90 s. Gels were formed upon cooling the solution to room temperature. A PBS solution was used for dilution to generate less concentrated gels. The gel layer was prepared by pouring a heated 3% agarose solution into a mold created using a glass slide with silicone gasket and trench (Grace Bio-Labs, OR). A second glass slide was then placed on top, enclosing the agarose, gasket, and trench between the two slides, which was then allowed to cool and harden. The glass slides were then removed and the gasket and trench were peeled away, leaving an agarose layer that is flat on both sides and has a trench down the middle. The wound model was assembled with a glass slide as a base, followed by the agarose layer, and then the PDMS layer. Each layer was simply placed on top of the other and held together by hydrophilic forces, completing the device (Fig. 1).

Experimental Setup

Solutions to be flowed were loaded into 1 mL syringes with 0.3 mm syringe tips and tubing (Becton, Dickenson and Company, Franklin Lakes, NJ). A syringe pump (Chemyx Fusion Touch, Stafford, TX) was used for constant flow rate. Tubing was put into the main inlet and outlet holes of the wound model and inserted through the agarose layer and down into the trench. A syringe filled with bacterial solution was attached and used to fill the trench, then the tubing was removed, and the holes were sealed with PDMS. On one side of the channel, arginine or glutamine at concentrations of 0.3 mM or 1 mM were flowed on one side, while PBS was flowed on the opposite side, creating an amino acid gradient. A video of the cellular activity inside the main channel was captured using a Nikon Eclipse Ti inverted microscope, a Nikon DS-QiMc microscope camera, and Nikon NIS Elements BR version 4.13 software (Nikon Instruments, Inc., Melville, NY). Microscope hardware settings consisted of an S Plan Fluor 40 \times objective in the phase contrast mode, equipped with NCB and D filters. The video was captured at 640 \times 512 resolution with a 60 ms exposure, 2 \times analog gain, and at 15 fps in 1-min long sections.

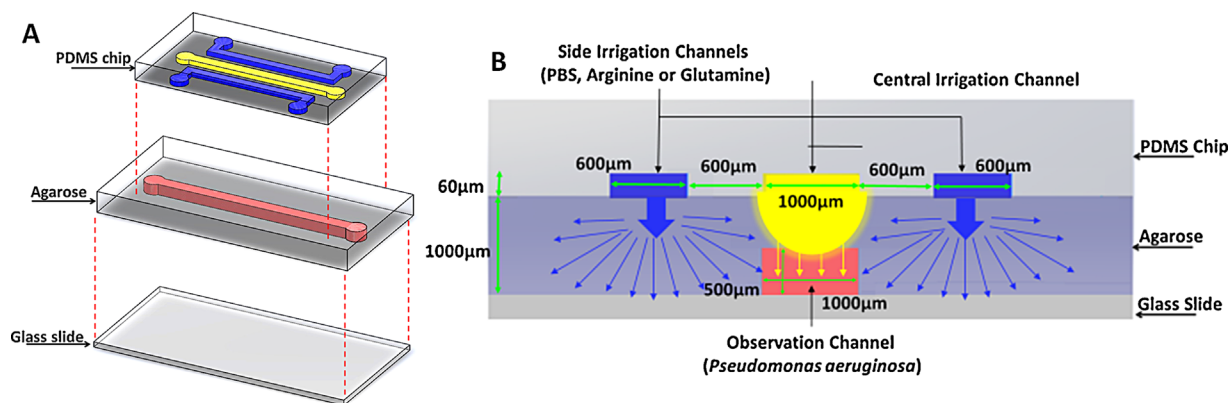


Figure 1. Schematic of the microfluidic 3D gradient generating wound model used for quantifying the interaction between *P. aeruginosa* and chemoeffector-releasing surfaces. **A:** The top layer is made of PDMS, which is impermeable to chemoeffector solutes. The middle layer is composed of agarose, which allows the diffusion of wound amino acids to establish the linear gradient profile. The observation channel has a depth of 500 μm . **B:** Illustration of the mechanism of gradient generation. Continuous flow of chemoeffector amino acids in the side irrigation channel and PBS solutions from the inlets of the PDMS mediates the formation of a gradient within the agarose layer and thus in the observation channel. Solid yellow lines and blue lines represent the entering of chemoeffectors from the sidewalls and the ceiling of the central observation channel, finally leaving through diffusion into the outlet channels.

Data Processing

The program ImageJ (<http://rsb.info.nih.gov/ij/>) was used for all video and image analysis. Captured videos were divided into 10 s segments and processed individually. To remove the background and non-motile cells, a projection of the entire video was used to create an average image that was used for flat field correction. A threshold was then applied to convert the video to binary data. Finally, the cells were tracked using the Manual Tracking Plugin (Fabrice Cordelières, Institut Curie, Orsay, France), and the raw data was exported to and processed using the Chemotaxis and Migration Tool (Ibidi Software, Munich, Germany). The two characteristics of cellular movement studied in this experiment are velocity and the forward migration index (FMI); the efficiency of motion in a given direction.

Device Characterization

To better understand the gradient generated by the microfluidic wound model, the apparent diffusion rates were characterized using 5 μm fluorescein (332.31 g/mol) and 5 μm Rhodamine B (479.02 g/mol); the movement of these fluorescent dyes could then be traced. The main channel of the device was filled with distilled water while one fluorescent solution was flowed into each side channel. Depending on the optical filter of the microscope at the time, the dyes could be viewed individually, showing the gradient moving from each side channel, allowing the diffusion rates to be tracked (Fig. 2). Results show that the diffusion and establishment of a proper gradient takes approximately 3–5 min and can vary depending on the flow rate.

Biofilm Growth Analysis

Static biofilm growth was measured using collagen coated and plain (non-coated) glass bottom cell culture dishes (Nunc, Thermo-scientific, Canada). To coat the culture dishes, a 75 $\mu\text{g}/\text{mL}$ type 1

rat-tail collagen (Sigma Chemical Co., St. Louis, MO) and 0.05 M hydrochloric acid solution was prepared, and 2 mL of it was placed in the culture dish, incubated for 2 h, and then washed with sterile water. Prepared bacterial solution was diluted to $\text{OD}_{600} = 0.05$, and 2 mL was placed in both the control and the collagen-coated cell culture dishes and then incubated for 4 and 24 h at 37°C. After incubation, the solution was gently removed using a pipette and then planktonic cells were washed away by tilting the culture dish, slowly flowing distilled water over top of it. The surfaces of the culture dishes were imaged using fluorescence optical microscopy, and five images of random surface areas were captured in each chamber. Dynamic biofilm growth was measured using a custom-built single channel microfluidic device. At the middle of the device, there is a shallow viewing area with supporting pillars designed to allow images or videos to be captured in high resolution and with all material in the device in one plane of focus (Fig. 3). This device was bonded to the agarose gel to create an enhanced surface microfluidic model.

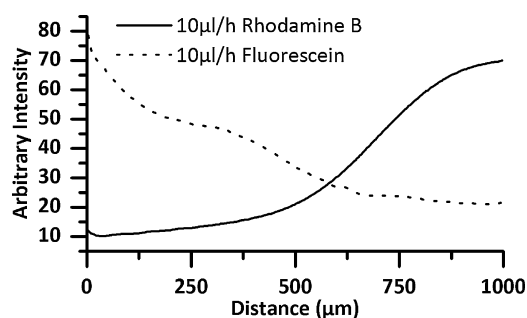


Figure 2. Temporal evolution of the chemoeffector concentration profile along the width of the observation channel of the microfluidic wound model.

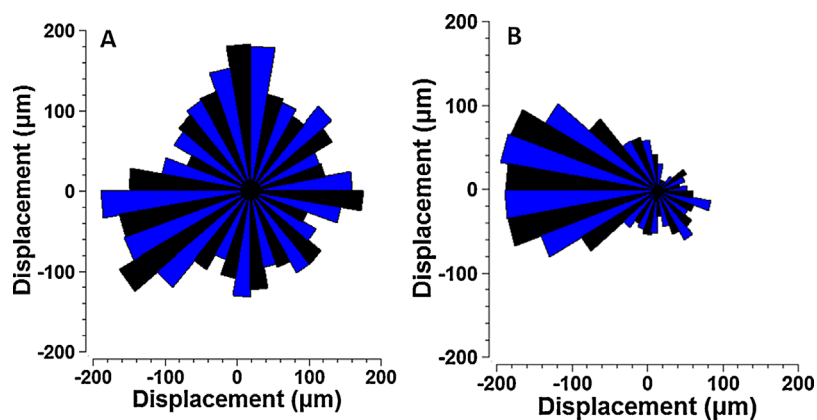


Figure 3. Differential chemotactic behaviour of GFP PAO1 to wound amino acids. Trajectories of GFP PAO1 (20 cells in each plot) when glutamine concentration is 0 (control) (A); 1 mM (B). In the chemoeffector experiment, glutamine was introduced in the left channel. Rose plots (A and B) demonstrate that cells migrated in all directions in the control but predominantly up the gradient in the chemoeffector experiment.

Confocal Laser Scanning Microscopy

Biofilms were imaged with an upright Leica DM RE microscope connected to a Leica TCS SP2 system with four different visible light lasers, covering six excitation wavelengths with a 63x (0.90 NA). Live bacteria were imaged using an excitation wavelength (Ex) of 488 nm and collecting emitted light in the “green” channel with a 514–535-nm window. Dead bacteria were imaged at Ex543 and collected in the “red” channel at 633 nm. There were only very few dead cells for modeling purposes, and hence only the green channel was used for acquiring the biofilm image. To characterize various aspects of the biofilm, 3D stacks were collected using several zoom settings and z-slices. To measure biofilm thickness, $OD_{600} = 0.05$ cell solutions were flowed through the single channel microfluidic device at $10 \mu\text{L/h}$ for 72 h. The inlet and outlets were sealed with wax, trapping the remaining solution and biofilm inside. Image stacks were taken of the biofilm at five different locations along the viewing channel of the microfluidic device using Confocal Laser Scanning Microscopy, and the biofilm thickness was measured using Leica Confocal Software (LCS, version 2.61).

Biofilm Co-Culture With *P. aeruginosa* and *E. coli*

E. coli (ATCC 700926) and *P. aeruginosa* (GFP-PAO1) were used in the mixed species biofilm study. Although most strains of *E. coli* are harmless, *E. coli* does cause infections. A study by Giacometti et al. (2000) on 676 patients with wounds identified *E. coli* as the third common bacterium causing serious infections followed by *P. aeruginosa* and *Staphylococcus aureus*. *E. coli* strain ATCC 700926 represents the bacterial human wound pathogen (Mølgaard et al., 2011). Stock cultures of *P. aeruginosa* and *E. coli* were streaked onto Luria–Bertani (LB) agar plates, and incubated for 72 h at 37°C . Single colonies of each strain were transferred into separate tubes containing 3 mL of sterile LB broth and grown overnight in a shaker at 37°C and 100 rpm for injecting into the microfluidic platform. The enhanced surface microfluidic platform model was injected

with 5 mL of diluted overnight culture containing approximately 1×10^8 CFU at a flow rate of $50 \mu\text{L/h}$ using a syringe pump (Harvard Apparatus, MA). Mixed species biofilms were established by inoculating mixed cultures of *E. coli* and PAO1 in a ratio of 1:1, which was optimized through previous experiments. Biofilm was allowed to grow 72 h inside the microfluidic platform for both the individual species and the mixed species experiments. *E. coli* cells were stained with SYTO 62 (Invitrogen) using a previously published protocol (Whitesides et al., 2001).

Statistical Analysis

All experiments were conducted in triplicate and repeated thrice. Quantitative data are represented by the mean value with the standard error of the mean. Statistical analysis was conducted using a paired *t*-test or unpaired, two-tailed *t*-test using Origin Pro software (Origin Lab, Northampton, MA). A significance value of $\alpha = 0.05$ was used for all tests.

Results

Development of a Robust Microfluidic System for Assessing Cellular Interactions in Polymicrobial Wound Environments

Structure-function relationships in the wound were considered in the design of our microfluidic platform to better emulate the mechanobiological nature of a wound infection. Nutrients and other biochemical cues are rarely constantly available in the wound environment, as the nutrient solution has to travel through porous networks of the collagen matrix before bacterial cells within a wound biofilm may access those (Fazli et al., 2011). This periodic availability of nutrients has been successfully mimicked in our wound model (Fig. 1), as the amino acids must travel through the agarose gel, which occurs at a slower flow rate due to diffusion as they pass through the porous network of the microfluidic platform.

With perfusion control, agarose-based gradient generation within the microfluidic platform better mimics the delivery of the amino acids and compounds in a wound microenvironment. The gradient of chemicals generated through the agarose present in our system resembles the network of spatial and osmotic chemical solution interactions inside the wound matrix (Zamierowski et al., 2010).

Bacterial swimming dynamics changes rapidly in response to either removal or addition of a specific chemoeffector, mainly due to the signaling components and sensory reception (Aizawa et al., 2000). By controlling diffusion gradient in the developed microfluidic model, it would be possible to influence the secretion and signaling patterns of the microorganisms present in the system. Soluble factor signaling within 3D agarose gel provides improved sensitivity with the ability to monitor the local concentration gradients surrounding the cells. The developed model helps to emulate various conditions present in the wound environment through the generation of concentration gradients within the agarose gel (Fig. 2). We can successfully track the spatial behavioral mechanisms of a single bacterial cell within its respective microscale resource landscapes. Initially, we generated a steady carbon source gradient by releasing arginine or glutamine from the sidewall of the porous agarose gel integrated into microfluidic platform (Fig. 1B), upon which individual cells would migrate toward the releasing surface. After switching arginine to PBS and reversing our setup, so release would occur at the opposite side wall, we observed that the cells changed their motility pattern and started migrating toward the other surface (Fig. 3). To understand the relationship between hydrodynamic conditions and biofilm growth, we used the microfluidic model platform with micro-posts (enhanced surfaces) on the surface (Fig. 4). Because of the gradient of the chemicals, temporal-spatial heterogeneity is considered in the construction of this device. Microbe-surface interactions play a critical role in biofouling, infection, and bioremediation, as surfaces can serve as a physical barrier that limit motility and dispersal; as nutrient hotspots in resource-limited environments; or as substrates as bacterial cells colonize and infect (Rusconi et al., 2014). In vivo-like micromechanical environment can be micro engineered for investigating cellular processes in pathophysiological contexts (Kim et al., 2009). Fluid shear stress is an important mechanostimuli as it can regulate bacterial cellular functions and may influence the attachment dynamics of bacteria to target cells (Thomas et al., 2002). The incorporation of

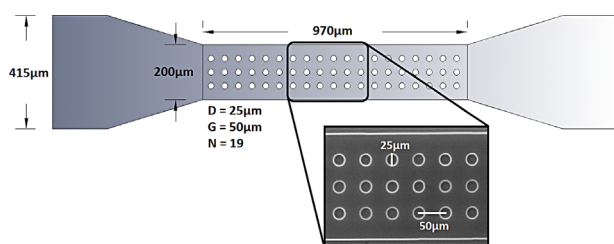


Figure 4. SEM image of the single-inlet microfluidic biofilm growth platform. The microfluidic chamber has a width of 200 μm , length of 970 μm , and a depth of 25 μm and is designed to fit on a standard glass cover slip.

microtopography geometries on the surface of the microfluidic platform provides cues along multiple axes for bacterial motility and for biofilm growth. In addition, the microposts offer shear forces that emulate the structural variations that can occur within 3D wound matrix. The micropost feature of the microfluidic platform was inspired by the lack of continuity found within in the natural wound tissue matrix (Vedula et al., 2013) and the relevant mesoscopic features of the general wound architecture.

Validation of a Non-Invasive Staining Technique for Labeling Individual Species in a Polymicrobial Biofilm

To validate the use of our model and pre-staining technique for the real-time monitoring of biofilm development, we compared the surface coverage of biofilms formed with the GFP-expressing strain to those formed with the wild type strain stained with SYTO 9. By measuring fluorescence intensity over time in chambers with the wild type or GFP-expressing strain, we were able to calculate the percent surface coverage for each, which is graphed as function of time in Figure 5. The percent surface coverage for the GFP-expressing strain may appear to be slightly greater than the surface coverage of the wild type strain when graphed as a function of time. However, these differences are not statistically significant; when acquiring images for both strains (from multiple positions in the chamber) at fixed time points (4 and 24 h), the differences were not significant ($P > 0.05$).

Looking at a single plane that reveals the topography of the chamber (Fig. 6A), we can clearly see that biofilm development is not uniform across the chamber, which reflects the natural heterogeneity of biofilms (Hall-Stoodley et al., 2009). Fluorescence intensity, reflecting cellular density, is greatest at the chamber edges where the shear flow forces are not as strong. The cells also appear to aggregate around the microposts of the microfluidic platform in areas where they might be better protected from shear forces. The optimum shear stress for the formation of biofilm at a flow rate of 10 $\mu\text{L}/\text{h}$ inside the microfluidic platform is 0.8 mPa, while the calculated shear stress surrounding the microposts was 0.5 mPa. Ultimately, this data shows that the hydrodynamic conditions within the system heavily influence the resulting biofilm architecture and cellular density. Therefore, careful modulation

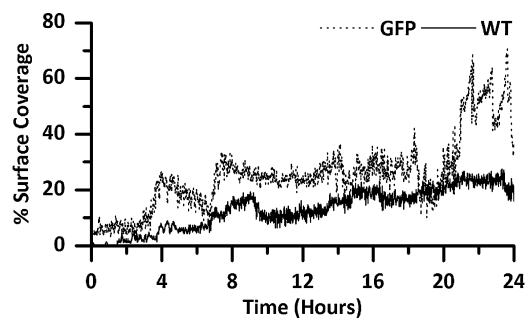


Figure 5. Area coverage of wild type and GFP-expressing *P. aeruginosa* bacterial biofilm grown on the surface inside the single channel microfluidic device at 10 $\mu\text{L}/\text{h}$ flow rate.

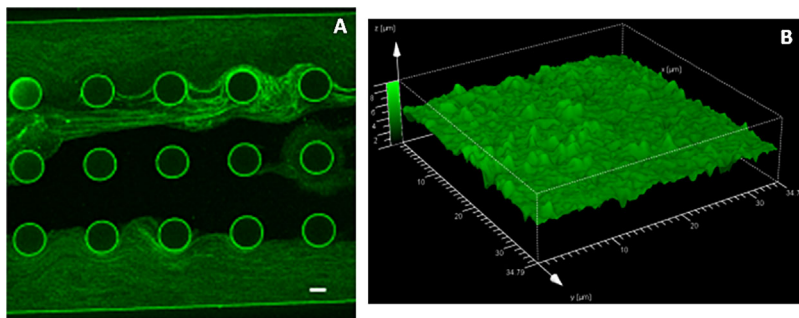


Figure 6. Growth and development of *P. aeruginosa* WT biofilms grown inside microfluidic channel platform (A) as observed by the Confocal Laser Scanning Microscopy at 72 h of growth showed in green channel. Scale bars equal 10 μ m. (B) 3D surface plot visualizations of wild type *P. aeruginosa* wild type, biofilms.

of this parameter should be implemented to mimic the conditions present in vivo. We also collected z-series of wild type biofilms for 3D reconstruction. Results of 3D modeling reveal that the biofilm possesses a distinct architecture that is not uniform across the surface of attachment (Fig. 6B). This unique 3D architecture and the accumulation pattern of both cellular and matrix biomass may ultimately influence the pathogenesis of our biofilms. The exopolysaccharide matrix modulates the interaction between the 3D architecture and virulence of a mixed-species biofilm (Xiao et al., 2012). The addition of nutrients or chemotactic stimuli may change this architecture, which can also be monitored using this approach.

Incorporation of Biologically Relevant Wound Materials and the Impact on Biofilm Formation

Although bacterial cells will attach to abiotic surfaces, it is important to incorporate relevant biological materials when modeling interactions occur in vivo. Using our new model, we tested the influence of collagen coating on the ability of *P. aeruginosa* to form biofilms. To evaluate the influence of collagen in a quantitative manner, we either coated slides with collagen or left them uncoated prior to the assembly of the microfluidic chamber. We then collected a series of images from random positions within each chamber that were used to calculate the percent surface coverage as described previously. We selected 4 h (early biofilm) and 24 h (late biofilm) time points for analysis. We found that at both early and late stages of biofilm formation, the addition of collagen resulted in a significant increase in the percent surface coverage of the biofilm (Fig. 7). Collagen coating influence early polymicrobial adhesive events (Birkenhauer et al., 2014). Our results emphasize the importance of conditioning or selecting an appropriate/relevant surface for attachment when evaluating biofilm formation.

Monitoring the Response of Biofilm Cells to Chemotactic Stimuli

To address an important and overlooked area of how nutrient source and availability influences the trajectory of biofilm development, we evaluated the impact of higher and lower doses of arginine and

glutamine on growing biofilms. Both of these amino acids can be metabolized by *P. aeruginosa*, are likely present at sites of wound infection, and have been long debated for their efficacy in speeding wound healing (Barbier et al., 2014). The concentrations range of aminoacids such as arginine and glutamine in a wound environment depends on several factors such as enzymatic pathways, healing stages, nutritional intake, and the values are typically in the range of micromolar concentrations (Witte et al., 2003). To assess the impact of amino acid introduction on *P. aeruginosa*, we measured the velocity (Fig. 8A) and FMI (Fig. 8B). We found that both presence and dose of amino acids had an impact on both factors. The addition of either amino acid at either concentration effectively reduced the velocity of the cells, while it increased the FMI (movement toward the amino acids). The higher concentration of arginine (1 mM) appeared to have the greatest impact on motility, which showed the slowest velocity among the four treatments. This suggests that both the presence and apparent concentration of arginine may dynamically influence motility. There

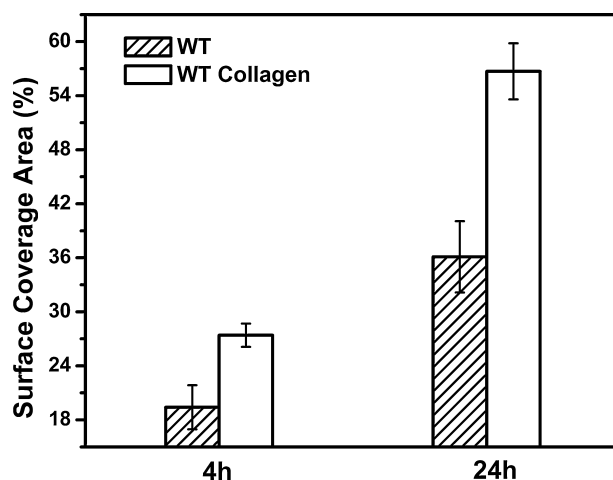


Figure 7. Accumulation of wild type (WT) *P. aeruginosa* biofilm on plain and collagen coated (GFP Collagen, WT Collagen) cell culture dishes over 4 and 24 h time points.

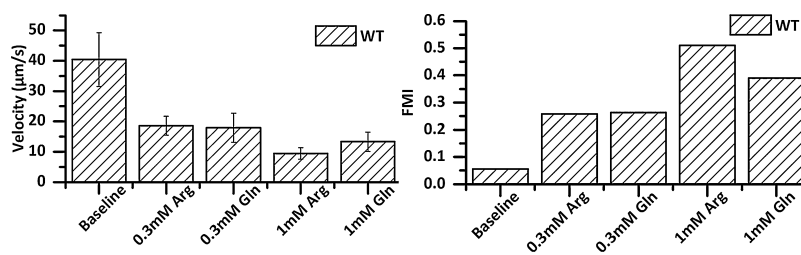


Figure 8. Migration of WT *P. aeruginosa* cells were measured in response to various concentrations of arginine (Arg) and glutamine (Gln) aminoacids in the microfluidic wound model observation channel. Baseline represents control experiment in the presence of buffer solution. Mean velocity is shown in (A) forward migration index (FMI) is shown in (B). Experimental data is reported as the average of 30 cells.

were no significant differences in motility between higher and lower doses of glutamine, which suggests that at this dose range at least, the concentration has less of an impact on motility. When looking at the FMI, again 1 mM arginine appeared to have the biggest impact, while there was no difference between higher and lower doses of glutamine, while all four treatments increased the FMI (movement toward chemotactic stimuli). Altogether, these data show that while overall motility is reduced in response to the introduction of amino acids, the cells are strongly attracted to both arginine and glutamine. The relationship between changes in motility to the chemotactic responsiveness is dependent on intracellular signaling processes and the bacterial strains. Interactions between chemoattractants and their receptors appear to affect the regulation of cell motility in response to starvation (Wei et al., 1998). CheR fluctuations increase motility but reduce chemotactic precision for *E. coli* bacterium (Matthaus et al., 2009). Regulators of cell polarity also play a role in directional sensing (Franca-Koh and Devreotes, 2004). The attraction toward these nutrient sources with a reduction in velocity may be indicative of a switch in lifestyle toward a sessile (biofilm) mode of growth where nutrients are plentiful.

Visualizing and Distinguishing Individual Species and Their Behaviors During Polymicrobial Biofilm Formation

Using a combination of a more traditional labelling approach (prior GFP tagging of the *P. aeruginosa* strain) and our new pre-labeling technique (SYTO 62 staining of *E. coli*), we were able to resolve the 3D architecture of dual-species biofilms formed with both organisms (Fig. 9). Ultimately, we were able to distinguish between red and green channels without significant overlap, indicating that our staining scheme is specific for each organism tested and that we are not detecting significant fluorophore cross-talk. At the same time, we can render each strain individually to examine their individual architectures or together to examine the overall biofilm architecture (Fig. 9A–C). It is apparent that the dual-species architecture is inherently more complex than single-species *P. aeruginosa* biofilms (Fig. 9C). We can clearly see individual *E. coli* (red) or *P. aeruginosa* (green) cells interacting with one another in single-plane cross-sectional images (Fig. 9D). Ultimately, these results demonstrate that our model is suitable for monitoring biofilm development for dual-species biofilms while still resolving individual cells and biofilm architectures to examine the structure as a whole and individually by

strain/cell. In the future, we plan to incorporate relevant stimuli (e.g., amino acids) to measure in real-time the response of individual cells within the complex polymicrobial environment to conditions relevant to the wound microenvironment. This data serves as an initial proof of principle that our model is adequate to conduct such studies of polymicrobial wound biofilms.

Discussion

Although it is now recognized that most bacterial pathogens exist in complex 3D environments that are influenced by both the host and resident organisms, very few models are available that accurately mimic the conditions present in vivo (Hall-Stoodley and Stoodley, 2009). In the course of our work, we have developed a model that can be used to culture at least two different relevant wound pathogens in a microenvironment that more closely mimics the natural wound environment, as demonstrated by our characterization of this system. Our approach is a significant technical innovation consisting of a two chamber system with a gradient through agarose which emulates the concentration gradient generation of chemoeffectors of the wound tissue layers. We also have validated a pre-culture labeling method that allows for the specific staining of individual species prior to biofilm initiation using commercially available and affordable stains that come in a variety of fluorophores. Pre-labeling is non-invasive and does not alter the resulting biofilm structure, while the results are similar to those obtained using a GFP-tagged strain. For applications where the construction of tagged strains may pose challenging (e.g., for clinical wound isolates that have not been genetically sequenced/characterized), this may prove to be a beneficial alternative. Furthermore, our system is adaptable, and we can incorporate relevant materials found at wound sites (e.g., collagen), as well as add nutrient sources and chemotactic stimuli during the course of culture to determine the direct impact of transient nutrient availability/concentration gradients on biofilm behavior.

The capability of our system to monitor the real time response to chemotactic agents is not trivial, as bacterial motility is a crucial factor in burn wound sepsis that contributes to colonization of the wound and dissemination from the site of infection. Gradient generation characterization experiments demonstrate that the developed system could serve as a potential assay for testing the interactions between pharmaceutical compounds, and the

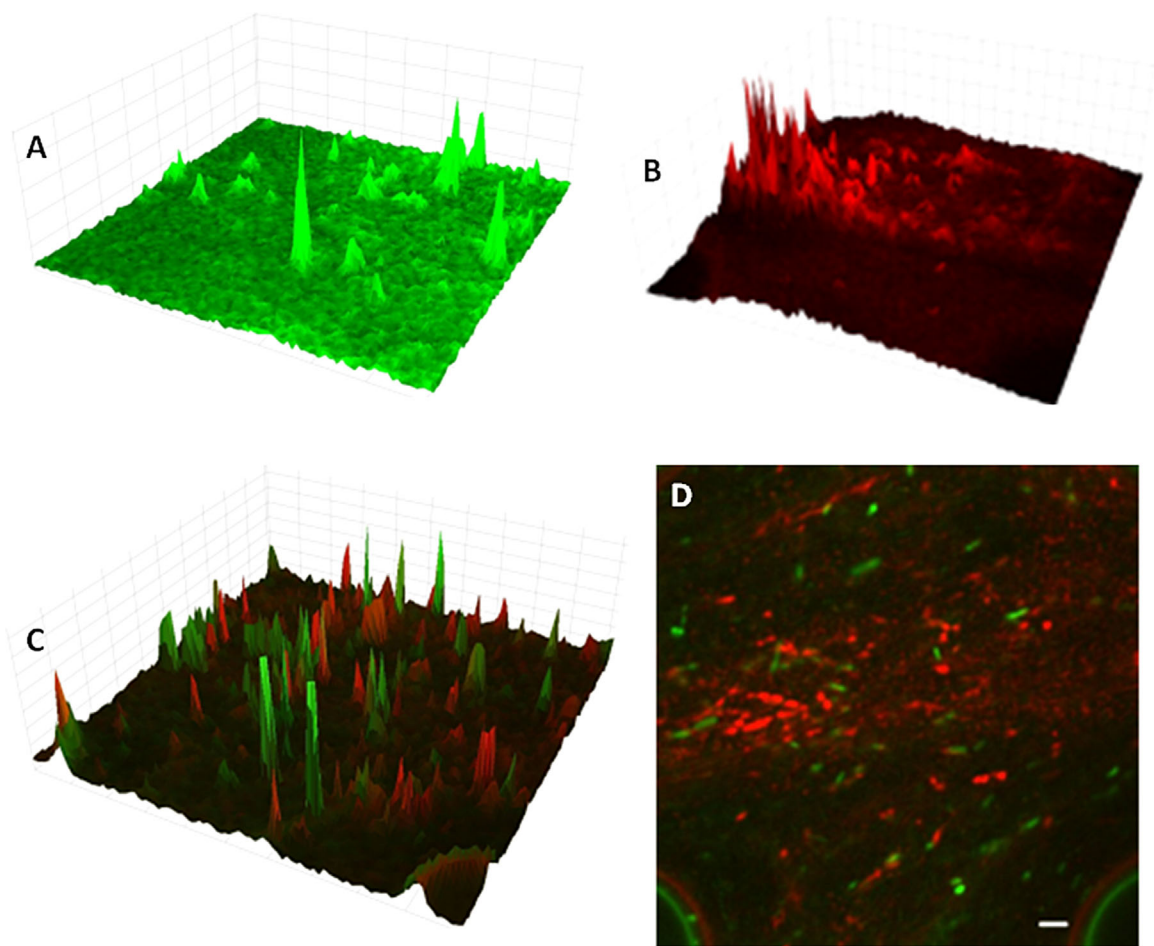


Figure 9. Spatial localization and structures of mixed-species biofilms grown inside the wound model microfluidic platform. Confocal Laser Scanning Microscopy (CLSM) 3D biofilm architecture of PAO1 (A) and *E. coli* (B). *P. aeruginosa* appears green and *E. coli* appears red. (C) Resulting mixed *P. aeruginosa*–*E. coli* biofilm inside the microfluidic platform. (D) Magnified view of a 2D segment of biofilm showing scattered patches of microcolonies of both PAO1 and *E. coli* and the co-species interactions. Scale bar equals 10 μm .

bacterium; and also to understand the polymicrobial interactions between bacterial species. The usage of fluorescent dyes to analyze chemoeffector concentration in the chamber addresses the aspects and relevance of diffusion gradient in the system that mimics the biology of the wounds. Our initial observations suggest that the administration of these amino acids slows motility while enhancing biofilm formation, which means that the administration of these amino acids may be detrimental to patient health by driving *P. aeruginosa* to form resistant biofilm structures. Our results clearly demonstrate that *P. aeruginosa* shows a chemotactic attraction to the tested amino acids. Additional study is warranted to pinpoint precise conditions for the application of amino acids to improve wound healing or to refute their use. Our data support the notion that exposure to arginine or glutamine helps *P. aeruginosa* to transition from a motile to a sessile, biofilm lifestyle. Differences in attachment and competitive or cooperative interactions with other residents of the wound environment may change the access to nutrients provided, altering the response. The biofilm micro-environment is complex, and likely no single model will be able to

address all the features of any given biofilm system. However, we have made significant steps forward in being better able to mimic the wound microenvironment. Our system is adaptable for use with various strains, even recent clinical isolates that have not yet been fully genetically characterized due to the implementation of microbial dyes that work for a wide range of organisms. Our characterization shows that we can successfully grow both *P. aeruginosa* and *E. coli* together and differentiate each species, while creating 3D reconstructions of their combined and individual architectures.

Conclusions

Classic microbiological approaches have relied upon the pure culture of individual species in batch culture; recent advances in microfluidic technology have led to the creation of systems that can be used to observe microorganisms in real-time in complex environments that more closely resemble their natural habitats. Microfluidic systems allows for the simultaneous culture of more

than one species with the application of relevant nutrient sources and materials found in vivo. To this end, we have devised a microfluidic platform that can be used to study interactions between organisms that are specific to the wound environment, as wounds are highly susceptible to colonization by resistant and harmful opportunist pathogens, such as *P. aeruginosa*. Our work represents a seminal step in establishing methodologies for the comprehensive study of the complex interactions that occur during wound infections with the ultimate goal of identifying new and selective therapeutic targets to control wound infections.

The authors thank the Natural Sciences and Engineering Research Council of Canada, and the Ontario Ministry of Research and Innovation for funding this study.

References

- Aizawa SI, Harwood CS, Kadner RJ. 2000. Signaling components in bacterial locomotion and sensory reception. *J Bacteriol* 182:1459–1471.
- Barbier M, Damron FH, Bielecki P, Suárez-Diez M, Puchałka J, Alberti S, Dos Santos VM, Goldberg JB. 2014. From the environment to the host: Re-wiring of the transcriptome of *Pseudomonas aeruginosa* from 22°C to 37°C. *PLoS ONE* 9:e89941.
- Birkenhauer E, Neethirajan S, Weese JS. 2014. Collagen and hyaluronan at wound sites influence early polymicrobial adhesive events. *BMC Microbio* 14:1–11.
- Fazli M, Bjarnsholt T, Kirketerp-Møller K, Jørgensen A, Andersen CB, Givskov M, Tolker-Nielsen T. 2011. Quantitative analysis of the cellular inflammatory response against biofilm bacteria in chronic wounds. *Wound Repair Regen* 19:387–391.
- Flemming H, Wingender J. 2010. The biofilm matrix. *Nat Rev Microbiol* 8:623–633.
- Franca-Koh J, Devreotes PN. 2004. Moving forward: Mechanisms of chemoattractant gradient sensing. *Physiol* 19:300–308.
- Giacometti A, Cirioni O, Schimizzi AM, Del Prete MS, Barchiesi F, D'errico MM, Petrelli E, Scalise G. 2000. Epidemiology and microbiology of surgical wound infections. *J Clin Microbiol* 38:918–922.
- Hall-Stoodley L, Costerton JW, Stoodley P. 2004. Bacterial biofilms: From the natural environment to infectious diseases. *Nat Rev Microbiol* 2:95–108.
- Hall-Stoodley L, Stoodley P. 2009. Evolving concepts in biofilm infections. *Cell Microbiol* 11:1034–1043.
- Jiricny N, Molin S, Foster K, Diggle SP, Scanlan PD, Ghoul M, Johansen HK, Santorelli LA, Popat R, West SA, Griffin AS. 2014. Loss of social behaviours in populations of *Pseudomonas aeruginosa* infecting lungs of patients with cystic fibrosis. *PLoS ONE* 9:1–10.
- Kim DH, Wong PK, Park J, Levchenko A, Sun Y. 2009. Microengineered platforms for cell mechanobiology. *Annu Rev Biomed Eng* 11:203–233.
- Kumar A, Karig D, Acharya R, Neethirajan S, Mukherjee PP, Retterer S, Doktycz MJ. 2013. Microscale confinement features can affect biofilm formation. *Microfluid Nanofluid* 14:895–902.
- Luckett JC, Darch O, Watters C, AbuOun M, Wright V, Paredes-Osses E, Ward J, Goto H, Heeb S, Pommier S, Rumbaugh KP, Camara M, Hardie KR. 2012. A novel virulence strategy for *Pseudomonas aeruginosa* mediated by an autotransporter with arginine-specific aminopeptidase activity. *PLoS Pathog* 8:e1002854.
- Matthäus F, Jagodič M, Dobnikar J. 2009. *E. coli* superdiffusion and chemotaxis—search strategy, precision, and motility. *Biophys J* 97:946–957.
- Mølgaard P, Holler JG, Asar B, Liberna I, Rosenbæk LB, Jebjerg CP, Jørgensen L, Lauritzen J, Guzman A, Adersen A, Simonsen HT. 2011. Antimicrobial evaluation of Huilliche plant medicine used to treat wounds. *J Ethnopharmacol* 138:219–227.
- Phillips PL, Wolcott RD, Fletcher J, Schultz GS. 2010. Biofilms made easy. *Wounds Int* 1:1–6.
- Rusconi R, Garren M, Stocker R. 2014. Microfluidics expanding the frontiers of microbial ecology. *Annu Rev Biophys* 43:65–91.
- Sackmann EK, Fulton AL, Beebe DJ. 2014. The present and future role of microfluidics in biomedical research. *Nature* 507:181–189.
- Sirianni RW, Kremer J, Guler I, Chen Y-L, Keeley FW, Saltzman WM. 2008. Effect of extracellular matrix elements on the transport of paclitaxel through an arterial wall tissue mimic. *Biomacromolecules* 9:2792–2798.
- Taylor GD. 2006. Training for renal ablative technique using an agarose-based renal tumour-mimic model. *BJU Int* 97:179–181.
- Taylor TB, Buckling A. 2010. Competition and dispersal in *Pseudomonas aeruginosa*. *Am Nat* 176:83–89.
- Thomas W, Trintchina E, Forero M, Vogel V, Sokurenko E. 2002. Bacterial adhesion to target cells enhanced by shear force. *Cell* 109:913–923.
- Togunde OB, Oakes K, Servos M, Pawliszyn J. 2012. Study of kinetic desorption rate constant in fish muscle and agarose gel model using solid phase microextraction coupled with liquid chromatography with tandem mass spectrometry. *Anal Chim Acta* 742:2–9.
- Turner KH, Everett J, Trivedi U, Rumbaugh KP, Whiteley M. 2014. Requirements for *Pseudomonas aeruginosa* acute burn and chronic surgical wound infection. *PLoS Genet* 10:e1004518.
- Tuson HH, Auer GK, Renner LD, Hasebe M, Tropini C, Salick M, Crone WC, Gopinathan A, Huang KC, Weibel DB. 2012. Measuring the stiffness of bacterial cells from growth rates in hydrogels of tunable elasticity. *Mol Microbiol* 84:874–891.
- Vedula SRK, Hirata H, Nai MH, Toyama Y, Trepast X, Lim CT, Ladoux B. 2013. Epithelial bridges maintain tissue integrity during collective cell migration. *Nat Mater* 13:87–96.
- Vedula SRK, Hirata H, Nai MH, Toyama Y, Trepast X, Lim CT, Ladoux B. 2013. Epithelial bridges maintain tissue integrity during collective cell migration. *Nat Mater* 13:87–96.
- Werthen M, Henriksson L, Jensen Ø P, Sternberg C, Givskov M, Bjarnsholt T. 2010. An in vitro model of bacterial infections in wounds and other soft tissues. *Apmis* 118:156–164.
- Whitesides GM, Ostuni E, Takayama S, Jiang X, Ingber DE. 2001. Soft lithography in biology and biochemistry. *Annu Rev Biomed Eng* 3:335–373.
- Witte MB, Barbul A. 2003. Arginine physiology and its implication for wound healing. *Wound Repair Regen* 11:419–423.
- Wright E, Neethirajan S, Warriner K, Retterer S, Srijanto B. 2014. Single cell swimming dynamics of *Listeria monocytogenes* using a nanoporous microfluidic platform. *Lab Chip* 14:938–946.
- Xiao J, Klein MI, Falsetta ML, Lu B, Delahunty CM, Yates JR, III, Heydorn A, Koo H. 2012. The exopolysaccharide matrix modulates the interaction between 3D architecture and virulence of a mixed-species oral biofilm. *PLoS Pathog* 8:e1002623.
- Zamierowski DS. 2010. Gradient wound treatment system and method. U.S. Patent No. 7,645,269. Washington, DC: U.S. Patent and Trademark Office.